Electronic Supplementary Material (ESI) for Journal of Materials Chemistry A.

Supporting Information

Effects of State Filling and Localization on Chemical Expansion in Praseodymium-Oxide Perovskites

Adrian Xiao Bin Yong[1, 2], Lawrence O. Anderson[1, 2], Nicola H. Perry[1, 2], and Elif Ertekin[*2, 3]

[1]Department of Materials Science and Engineering, University of Illinois Urbana-Champaign, Urbana, Illinois, USA

[2]Materials Research Laboratory, University of Illinois Urbana-Champaign, Urbana, Illinois, USA

[3]Department of Mechanical Science and Engineering, University of Illinois Urbana-Champaign, Urbana, Illinois, USA

[*]Corresponding author; Email: ertekin@illinois.edu

The projected density of states (PDOS) of stoichiometric $PrGaO_3$ and $BaPrO_3$ are as shown in Fig. S1. Note that the energies of each plot have been shifted such that the Fermi level is located at 0 eV. As the U value increases, the occupied Pr-4f states shift left towards the O-2p states, whereas the unoccupied Pr-4f states shift right towards the Pr-5d states.

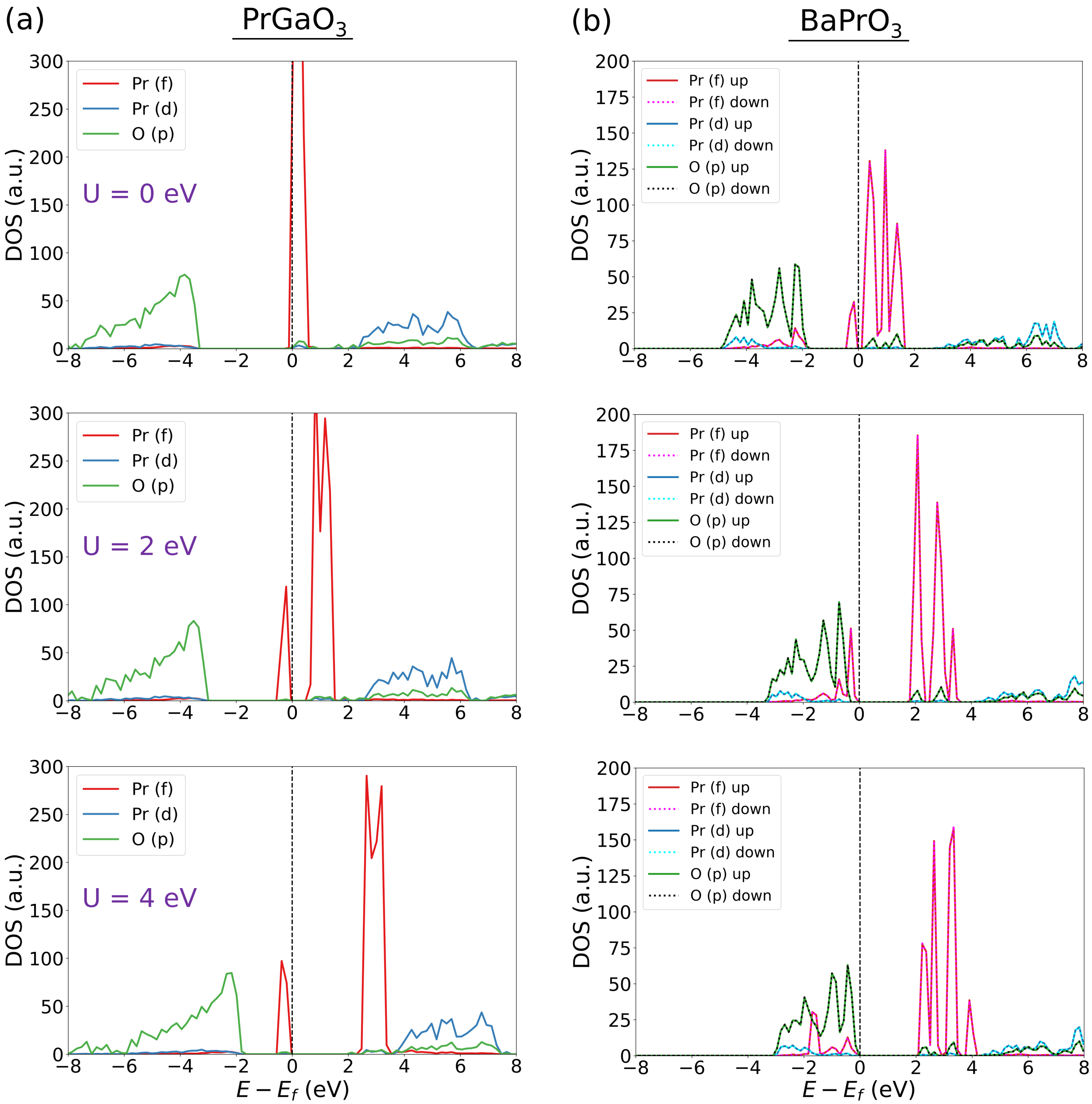

Figure S1: Calculated PDOS of (a) $PrGaO_3$ and (b) $BaPrO_3$ for $U = 0$, 2, and 4 eV. The black dashed line represents the Fermi level.

The PDOS of $\mathrm{PrGa_{0.875}Mg_{0.125}O_{3-\delta}}$ (PGM) for $\delta = 0$ and 0.0625 are as shown in Fig. S2. For $U = 2$ eV, the inset shows the enlarged PDOS of the F'-center defect state formed when an O vacancy is introduced to the supercell, which is lower in energy than the Pr-4f hole states.

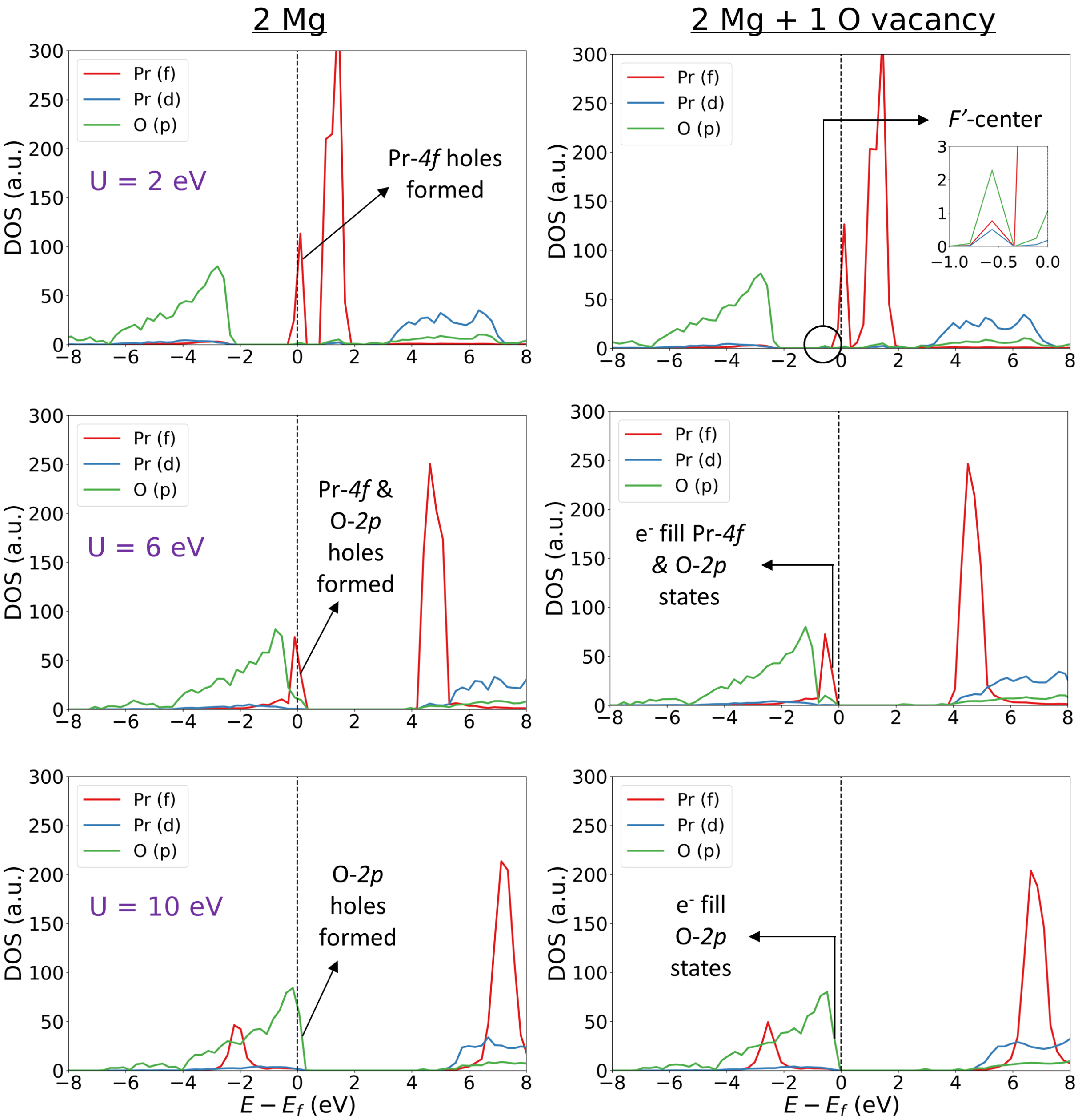

Figure S2: Calculated PDOS of PGM for the supercell with 2 Mg dopants atoms introduced and the supercell with an additional O vacancy added for $U = 2$, 6, and 10 eV. All results are shown for the arrangement where the Mg atoms and O vacancy are far apart. The PDOS of states not shown are negligible in the energy range of the plots.

Table S1 shows the energy difference between the arrangement where the defects are far apart (E_{far}) and the arrangement where the defects are close together (E_{close}) for PGM. Note that the O vacancy was placed far from both Mg dopant atoms in the far arrangement, and between the Mg dopant atoms in the close arrangement. When there are no O vacancies present in PGM, the far arrangement is more energetically favorable by ∼1 eV per pair of dopants than the close arrangement, as the latter leads to higher strain. When an O vacancy is introduced to PGM, the energy difference decreased to ∼0.2 eV due to the favorable association between $\mathrm{Mg}'_{\mathrm{Ga}}$ and $\mathrm{v}_{\mathrm{O}}^{\bullet\bullet}$. However, the far arrangement remained more energetically favorable suggesting that strain effects outweigh the favorable association between the Mg dopants and the O vacancy. If a third case is considered where the Mg dopants are far apart but the O vacancy is located next to one of the Mg dopants, this arrangement will likely be more energetically favorable than the arrangement where all defects are far apart.

Table S1: Energy difference between the far and close arrangements of defects for PGM, when the O vacancy is absent or present

	$E_{far} - E_{close}$ (eV)	
U (eV)	No O vacancy	1 O vacancy
4	−0.860	−0.170
6	−0.926	−0.250
8	−0.984	−0.233
10	−0.987	−0.236

The PDOS of $\mathrm{BaPrO}_{3-\delta}$ (BPO) for $\delta = 0$ and 0.0625 are as shown in Fig. S3.

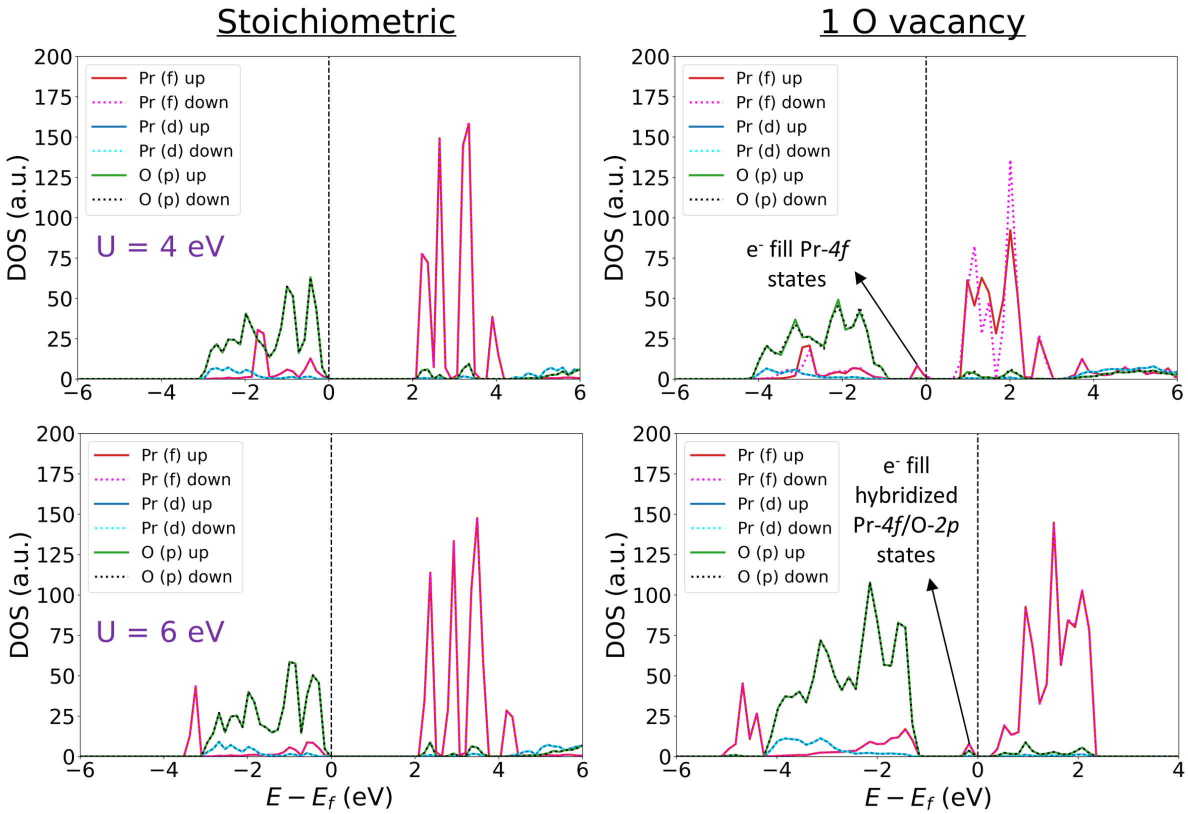

Figure S3: Calculated PDOS of BPO for the supercell with no O vacancy (stoichiometric) and the supercell with one O vacancy added for $U = 4$ and 6 eV. The repeated calculations of BPO for each U value generally yield similar PDOS as shown here.

The PDOS of $\mathrm{BaPr_{0.875}Y_{0.125}O_{3-\delta}}$ (BPY) for $\delta = 0$ and 0.0625 are as shown in Fig. S4.

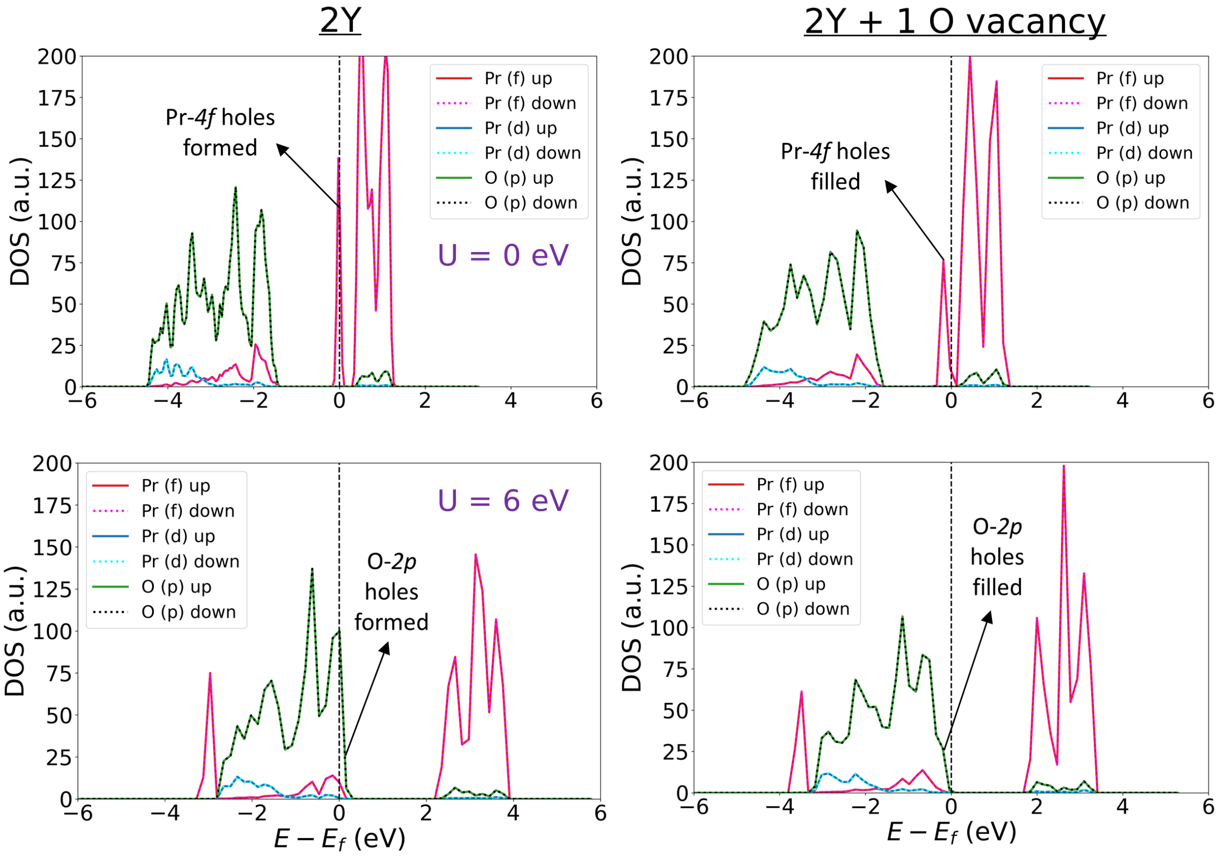

Figure S4: Calculated PDOS of BPY for the supercell with 2 Y dopants atoms introduced and the supercell with an additional O vacancy added for $U = 0$ and 6 eV. All results are shown for the arrangement where the Y atoms and O vacancy are close together.

Supplementary Note 1. Pr-3*d* XPS spectra fitting

Quantitative determination of the $\mathrm{Pr}^{3+}/\mathrm{Pr}^{4+}$ ratio in the surface of our materials requires fitting of the XPS data. In literature concerning Pr oxides, different fitting approaches have been applied[1–3], which for our compositions and data yield different ratios. To our knowledge, two primary fitting approaches have been presented: Method 1[1] has been used to determine the amount of Pr^{4+} impurity ions in a $\mathrm{Pr}_x\mathrm{La}_{1-x}\mathrm{AlO}_3$ solid solution. Method 2[2,3] has been used for Pr-doped $\mathrm{In}_2\mathrm{O}_3$, and two-phase composites composed of a (La,Sr,Pr)CoO_3 perovskite phase and a $(\mathrm{La,Sr,Pr})_2\mathrm{CoO}_4$ Ruddlesden–Popper phase. However, to the best of our knowledge, neither method has been used to track changes in Pr valence with fixed valence cation substitution or with changes in partial pressure of oxygen (pO2), where the change in Pr valence can be reliably predicted in these cases and the validity of the fitting method can be assessed. Also, neither method has been compared to complementary experimental techniques to verify the valence state(s) of Pr.

Figure S5 shows our Pr-3*d* spectra fitted using Method 1 and Method 2. Method 1 assigns the $4f^2$ and $4f^3\underline{L}$ peaks as Pr^{3+}, and the $4f^1$ peaks as Pr^{4+}. Although the $4f^1$ peaks indicate the presence of Pr^{4+}, the $4f^2$ and $4f^3\underline{L}$ peaks may also receive a contribution from Pr^{4+} (instead of Pr^{3+} only). Method 2 allows the $4f^2$ and $4f^3\underline{L}$ peaks to have contributions from both Pr^{3+} and Pr^{4+}, and the peaks are assigned according to the relative peak positions of reference oxides $\mathrm{Pr}_2\mathrm{O}_3$ (Pr^{3+}) and PrO_2 (nominally Pr^{4+}). However, PrO_2 is inappropriate as a reference for Pr^{4+} due to covalency in the Pr–O bonding[4]. Furthermore, binding-energy shifts of around 1 eV are present between the Pr-3*d* spectra of PGM/BPY and the reference oxides, where similar binding-energy shifts (0-1.5 eV) were observed in other mixed Pr oxides[1–3,5,6]. These binding-energy shifts may be caused by differences in bond covalency, Madelung energy, and/or final-state relaxation effects[7]. These significant shifts make the identification of the (up to) 10 highly convoluted peak positions for Pr^{3+} and Pr^{4+} challenging, where Method 2 uses a strict adherence to the relative peak positions of the reference oxides to quantify Pr^{3+} and Pr^{4+}. Also, Method 2 restricts the full width at half maximum (FWHM) to 2.4-2.6 eV. Both methods maintain the area ratio of 1:0.66 for the $3d_{5/2}$ and $3d_{3/2}$ peaks.

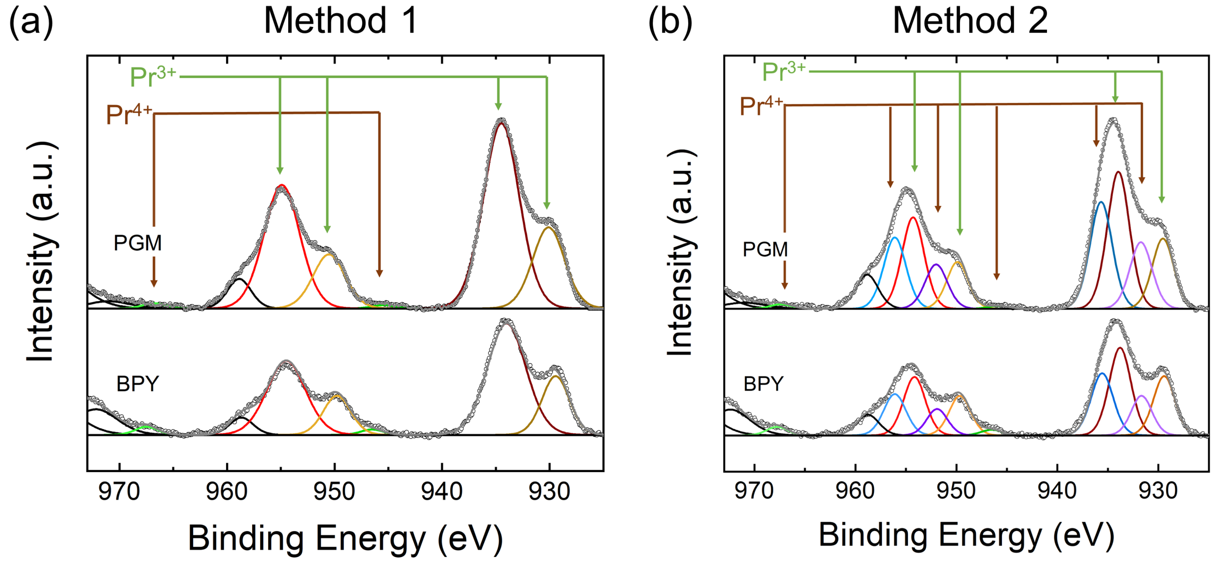

Figure S5: Pr-3*d* XPS spectra of PGM and BPY fitted using (a) Method 1 and (b) Method 2. Note that the region between 970-980 eV is attributed to O KLL Auger emissions[1,8].

The fractions of Pr^{3+} and Pr^{4+} ions were calculated from the fitted peak areas according to Ref. 2 (FWHM fixed to 2.45 eV), and the results for both methods are summarized in Table S2. Method 1 results in mostly Pr^{3+} for both materials, with a slightly higher Pr^{4+} fraction for BPY. However, the Pr^{4+} fraction still appears to be unusually low for BPY, even after taking into account the Pr–O bond covalency in BPY. On the other hand, Method 2 results in much higher Pr^{4+} fractions for both materials, and actually shows a higher Pr^{4+} fraction for PGM than for BPY. The fraction of Pr^{4+} in PGM is unreasonably high, since Pr should exist as mostly Pr^{3+} in PGM. Neither fitting method appears to give valence fractions that we can confidently rely on without further experimental verification using methods such as X-ray absorption spectroscopy (XAS). Hence, we chose to perform only a qualitative comparison of the raw spectra instead of using fitted results.

Table S2: Pr^{3+} and Pr^{4+} fractions of PGM and BPY, determined from the Pr-3d spectra fitted using Methods 1 and 2

Material	Fitting method	Pr^{3+} fraction	Pr^{4+} fraction
PGM	Method 1	0.987	0.013
	Method 2	0.540	0.460
BPY	Method 1	0.969	0.031
	Method 2	0.572	0.428

Supplementary Note 2. Comparison between XPS valence spectra and DOS

Since we do not observe an isolated (Pr-4f) peak located to the right of the broad (O-2p) feature near the Fermi level of the XPS valence spectra, this indicates that appropriate descriptions of PGM and BPY in DFT+U require $U \geq 6$ eV and $U \geq 2$ eV respectively. For these ranges of U values, there is generally good agreement between the XPS valence spectra and the calculated density of states (DOS). Since comparisons were made with the DOS directly without conversion into simulated XPS spectra, some differences in peak widths (peak broadening effects[9] are present in experiments) and peak intensities (the photoelectron spectrum is dependent on the orbital cross sections and excitation energy[10]) are expected. The feature at around 12 eV in the BPY XPS spectrum corresponds to the beginning of the Ba-5p peak. However, the small peak at around 9 eV in the BPY XPS spectrum is not present in the calculated DOS. This peak is unlikely to be the Pr-4f peak since photoelectron spectroscopy data of $BaPrO_3$ from literature[11,12] reported Pr states to be located near the top of the O states in the valence band. This discrepancy may have been due to XPS being a surface sensitive technique (∼5 nm), whereas the calculated DOS was for the bulk. The coordination environment and possibly composition could be different between the surface and the bulk. Furthermore, BPY was modelled as antiferromagnetic[13] in DFT (0 K), but it should lose its antiferromagnetic ordering at room temperature. These potential differences in surface composition/coordination and magnetism may have led to the observation of the additional peak in the XPS spectrum. However, this peak is far enough below the valence band maximum that it should not influence the formation/location of holes.

Calculations of stoichiometric $PrGaO_3$ and $BaPrO_3$ were also performed using the Heyd-Scuseria-Ernzerhof (HSE06) hybrid functional[14]. The orbitals were expanded using a plane wave basis with cutoff energy of 520 eV for both materials. $PrGaO_3$ was calculated using its unit cell, and the Brillouin zone was sampled using a $(3 \times 3 \times 3)$ gamma centered k-point grid. $BaPrO_3$ was calculated using $2 \times 2 \times 2$ unit cells, initialized with a G-type antiferromagnetic ordering[13], and the Brillouin zone was sampled using a $(2 \times 2 \times 2)$ Monkhorst-Pack k-point grid. Structural relaxations were performed, allowing the cell shape, cell volume, and atom positions to relax, until the force on each atom was below 0.01 eV/Å.

The PDOS for both materials are as shown in Fig. S6. Based on the relative positions of the Pr-4f and O-2p states in the valence band, the PDOS calculated using HSE06 appear to match those calculated using PBE and $U = 4$ eV for both PGO and BPO (see Fig. S1), apart from the underestimated band gap for PBE. Although the Hubbard U correction was only applied to the Pr-4f states in PBE+U, the Pr-5d states still match well with HSE06 and do not appear to be overly delocalized. Our experimental valence band XPS spectra showed that the Pr-4f peak in the valence band is not an isolated peak located to the right of the O-2p states, indicating that HSE06 still does not describe $PrGaO_3$ correctly despite being a higher level of theory.

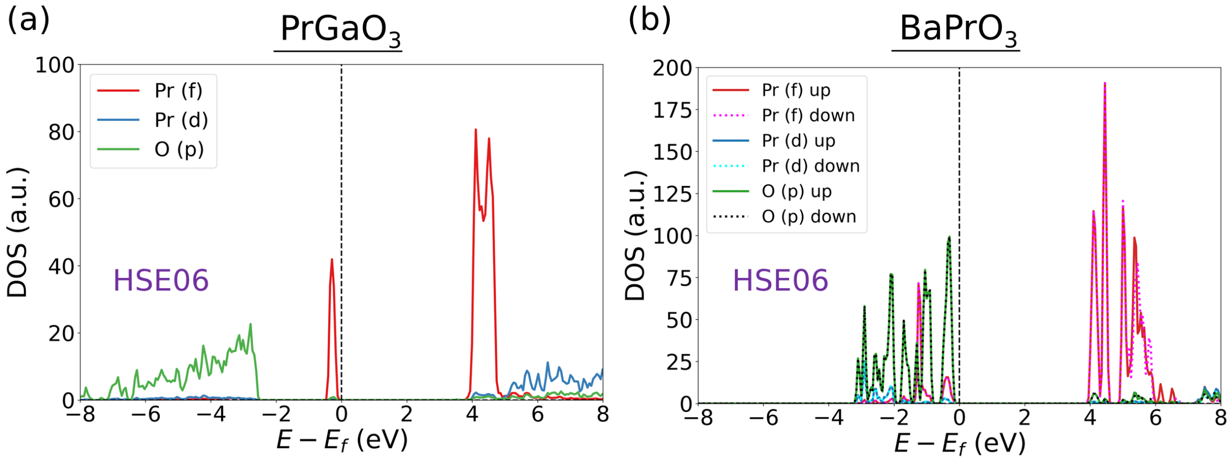

Figure S6: Calculated PDOS of (a) $PrGaO_3$ and (b) $BaPrO_3$ using the HSE06 hybrid functional.

The strain along the *a*-, *b*-, and *c*-axis for PGM when one O vacancy is introduced is shown in Fig. S7. PGM is orthorhombic and demonstrates an anisotropic chemical expansion, where the expansion is the largest along the *a*-axis, followed by the *c*-axis, and is accompanied by a contraction along the *b*-axis. This anisotropic expansion is consistent across all U values regardless of which hole states are filled, and matches our previously reported experimental measurements[15].

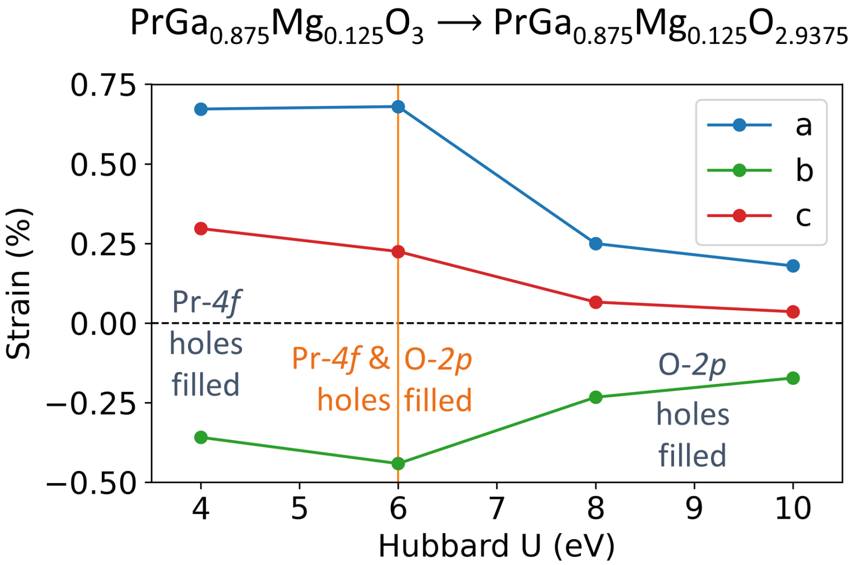

Figure S7: Plot of percentage strain as a function of Hubbard U for introducing one O vacancy to $PrGa_{0.875}Mg_{0.125}O_3$.

References

[1] M. Szubka, E. Talik, A. Molak, S. Turczyński and D. A. Pawlak, *Crystal Research and Technology*, 2010, **45**, 1309–1315.

[2] E. Y. Konysheva and M. V. Kuznetsov, *RSC Advances*, 2013, **3**, 14114–14122.

[3] J.-S. Kim, C. W. Na, C.-H. Kwak, H.-Y. Li, J. W. Yoon, J.-H. Kim, S.-Y. Jeong and J.-H. Lee, *ACS Applied Materials Interfaces*, 2019, **11**, 25322–25329.

[4] S. G. Minasian, E. R. Batista, C. H. Booth, D. L. Clark, J. M. Keith, S. A. Kozimor, W. W. Lukens, R. L. Martin, D. K. Shuh, S. C. E. Stieber, T. Tylisczcak and X.-d. Wen, *Journal of the American Chemical Society*, 2017, **139**, 18052–18064.

[5] S. K. Pandey, R. Bindu, P. Bhatt, S. M. Chaudhari and A. V. Pimpale, *Physica B: Condensed Matter*, 2005, **365**, 47–54.

[6] E. Poggio-Fraccari, G. Baronetti and F. Mariño, *Journal of Electron Spectroscopy and Related Phenomena*, 2018, **222**, 1–4.

[7] M. J. Guittet, J. P. Crocombette and M. Gautier-Soyer, *Physical Review B*, 2001, **63**, 125117.

[8] B. Demri and D. Muster, *Journal of Materials Processing Technology*, 1995, **55**, 311–314.

[9] P. S. Bagus, E. S. Ilton and C. J. Nelin, *Surface Science Reports*, 2013, **68**, 273–304.

[10] M. Bagheri and P. Blaha, *Journal of Electron Spectroscopy and Related Phenomena*, 2019, **230**, 1–9.

[11] T. Higuchi, A. Oda, T. Tsuchiya, T. Suetsugu, N. Suzuki, S. Yamaguchi, M. Minohara, M. Kobayashi, K. Horiba and H. Kumigashira, *Journal of the Physical Society of Japan*, 2015, **84**, 114708.

[12] S. Furuichi, T. Tsuchiya, K. Horiba, M. Kobayashi, M. Minohara, H. Kumigashira and T. Higuchi, *Transactions of the Materials Research Society of Japan*, 2017, **42**, 15–18.

[13] N. Rosov, J. W. Lynn, Q. Lin, G. Cao, J. W. O'Reilly, P. Pernambuco-Wise and J. E. Crow, *Physical Review B*, 1992, **45**, 982–986.

[14] A. V. Krukau, O. A. Vydrov, A. F. Izmaylov and G. E. Scuseria, *The Journal of Chemical Physics*, 2006, **125**, 224106.

[15] L. O. Anderson, A. X. B. Yong, E. Ertekin and N. H. Perry, *Chemistry of Materials*, 2021, **33**, 8378–8393.